Journal of Power Sources 232 (2013) 29–33

Contents lists available at SciVerse ScienceDirect

Journal of Power Sources

journal homepage: www.elsevier.com/locate/jpowsour

Short communication

On the stress characteristics of graphite anode in commercial pouch lithium-ion battery

Dongren Liu [a,*], Ying Wang [a], Yuansen Xie [a], Liping He [a], Jie Chen [a], Kai Wu [a], Rui Xu [a], Yan Gao [b]

[a] Dongguan Amperex Technology Limited, Dongguan 523808, PR China
[b] School of Materials Science and Engineering, South China University of Technology, Guangzhou 510640, PR China

HIGHLIGHTS

- The stress of graphite anode in pouch cell is characterized.
- Compressive stress inhomogeneously distribute in graphite anode.
- Stress generates and accumulates in the early stage of cycling process.
- Stress of graphite anode is directly related to cell thickness swelling.
- Stress causes fast capacity fading during cycling process.

ARTICLE INFO

Article history:
Received 21 September 2012
Received in revised form
11 December 2012
Accepted 19 December 2012
Available online 11 January 2013

Keywords:
Micro-Raman mapping
Stress
Graphite anode
Pouch lithium-ion battery

ABSTRACT

The stress of graphite anode in commercial pouch lithium-ion battery is characterized ex-situ by using micro-Raman mapping technique at 2 μm lateral resolution. The results show that the stress in graphite anode is always compressive and its distribution is inhomogeneous both in the manufacturing process and in cycling process. The stress mainly generates and accumulates in the early stage of cycling process, which causes not only big anode thickness swelling but also graphite particles cracking or even degrading. The deterioration of electrical contact of graphite particles from current collector caused by anode volume expansion and formation of solid electrolyte interface (SEI) in fresh surface of cracked graphite particle is responsible for the faster capacity fading of pouch battery in this early stage.

1. Introduction

When lithium-ion battery (LIB) undergoes charge and discharge cycling, the intercalation/extraction of lithium ions into/from the graphite lattice causes repeated expansion and contraction of graphite particle. Stresses are inevitably generated in anode by such periodic volume change and are probably accumulated in cycling process. Stress is also introduced into anode during the manufacturing process such as calendering. Although the capacity fading mechanism of graphite anode has been intensively studied [1–3], the correlation of stress characteristic of graphite anode with its capacity loss is not well understood yet. Furthermore, as ultra-thin consumer electronic devices such as mobile phone and laptop PC become increasingly favorable, the space within those thin devices for accommodating power source is strictly limited. For pouch LIB equipped in those thinner devices, the stress of anode would lead to undesirable volume expansion, which is regarded as a potential damage to the delicate electrical unit. It becomes more and more significant to understand the stress characteristics in graphite anode so as to prolong the cycle life and reduce the volume expansion of commercial pouch battery.

Many efforts have been devoted to understand the stress in graphite anode by numerical simulation [4–8]. Most of those simulations considered the stress of single graphite particle caused by the lithium-ion concentration gradient from graphite particle surface to its interior. However, the porous and composite structure of graphite anode was neglected less or more. So, the validity of those results predicted by the simulation studies should be verified practically in the commercial battery. In-situ analyses of anode stress during lithium-intercalation/extraction have been reported by several groups [9–11]. Those in-situ stress measurements were mostly based on a cantilever beam-bending method, in which curvature of

* Corresponding author. Tel./fax: +86 769 88989132.
E-mail address: Liudr@atlbattery.com (D. Liu).

0378-7753/$ – see front matter © 2013 Elsevier B.V. All rights reserved.
http://dx.doi.org/10.1016/j.jpowsour.2012.12.110

the substrate is monitored by laser beam and is used to calculate stress in a film deposited on it through the Stoney equation. However, this method will lose its ability on stress measurement in prolonged charge–discharge cycling because the substrate fatigue and plastic deformation will take place after hundreds of expansion and contraction. On principle, this method cannot provide detailed stress distribution in a film but overall stress parallel to the substrate. As reported in literature [12–17], micro-Raman spectroscopy (MRS) is a powerful technique for stress characterization. Although ex-situ micro-Raman mapping cannot precisely monitor the real-time stress variation during one or several charge–discharge cycles, it can probe credibly the stress characteristic in static state during prolonged charge–discharge cycling because the MRS measurement is not based on the substrate but on the graphite particle itself. The other advantages of ex-situ micro-Raman mapping over those in-situ methods lie in the capability of mapping the stress distribution and the convenience on sample preparation. In this work, we report an ex-situ stress analysis of graphite anode by using this MRS method, with the aim of understanding the stress characteristic and variation of graphite anode in commercial pouch cell during the manufacturing and prolonged cycling process.

2. Experimental

The graphite anode was prepared by a well-established industrial procedure. In brief, commercial graphite powder, styrene–butadiene rubber, carboxymethyl cellulose, and water were severely blended to form homogeneous slurry, which was then coated on a thin Cu foil by a transfer coating technique. After drying and calendering, the porous composite graphite anode was cut to strips and then baked at 120 °C under vacuum. The graphite anode, $LiCoO_2$ cathode, and PE separator were wound together and subsequently sealed with an aluminum laminate film package to assemble pouch cell. The electrolyte injected into cell is made up of $LiPF_6$ dissolved in hybrid carbonate solvent comprising of EC, PC, EMC and additives. At first, the as-manufactured cell was galvanostatically charged to form a stable SEI on graphite surface. Then the cell was charged to 4.2 V and its thickness and resistance are measured. The cell thickness was measured with a home-made Parallel Plate Gauge, in which two parallel plates are coupled with a micrometer. By placing the cell between those two parallel plates in this gauge, the cell thickness was gained. The cell resistance was derived by measuring the AC impedance at 1 kHz frequency between anode and cathode using a battery internal resistance tester. The cells were continuously charged and discharged in the voltage range between 3.0 V and 4.2 V for hundreds of cycles with a charge/discharge current of 1.4 A/1.0 A (cell capacity: 2 Ah) at 45 ± 1 °C. Every 50 charge/discharge cycles, the thickness and resistance of the cells at 4.2 V were measured. During the cycling, the cells undergone 100, 200, and 350 charge/discharge cycles were picked out and subsequently fully discharged to 2.8 V with a current of 20 mA to completely remove Li ion from graphite lattice. The as-discharged cell was disassembled and the graphite anode was dried under vacuum for 4 h at ambient temperature for MRS test.

A confocal Raman spectroscopy instrument (LabRAM Aramis, Horiba Jobin Yvon) was used to detect the Raman spectrum of dried graphite anode. The excitation wavelength was supplied by a He–Ne (633 nm) radiation which was calibrated by standard polycrystalline silicon sample (99.99% purity) before test. The power of the laser beam was adjusted to 0.1 mW with neutral filters and the irradiation time of laser on sample is 10 s. The radius of the laser spot on the graphite anode surface was about 1 μm (100× objective). Micro-Raman mapping of the anode surface was carried out across 30 μm × 30 μm area at 2 μm lateral resolution. The Raman spectra were collected in the wavenumber range from 1200 cm^{-1} to 1800 cm^{-1} and the recorded spectra were fitted with Gauss–Lorentz mixed-function using commercial software (SpectraCal, Galactic Industries).

3. Results and discussion

3.1. Stress characterization of graphite anode in pouch LIB

The first-order Raman spectrum of graphite includes two peaks: G peak (ca.1580 cm^{-1}) and D peak (ca.1350 cm^{-1}) [18]. G peak originates from E_{2g} phonons among the zone center modes of graphite sheet. D peak is generally supposed to be induced by the disorder associated with finite crystallites sizes. The peak intensity ratio I_D/I_G is often used to determine the extent of structural disorder (e.g., $I_D/I_G = 0$ for a perfect, infinite graphene layer) in graphite and/or the size of the graphitic domains. Many previous works revealed that the characteristic Raman peak shifts of various crystal materials such as Si [12–17], alumina [12], and SiC [19] are linearly dependent upon macroscopically applied uniaxial stress. The Raman peak position tends to move linearly to lower wavenumber under tensile stress and to higher wavenumber under compressive stress. For graphite powder, the exactly quantitative dependence of its peak shift upon the stress is not obtained at present due to the difficulty on imposing uniaxial stress on micro-scaled particle and simultaneously measuring its Raman spectrum under stress. However, as a member of graphite family, carbon fiber was reported to show linear dependence of G peak shift on uniaxial stress [20,21]. Accordingly, G peak shift of graphite powder is assumed to be linearly dependent on the magnitude and direction of stress in graphite anode in this work.

The G peak shift of stressed graphite anode, which is considered to be proportional to the stress of graphite anode, is denoted by the wavenumber difference ($\Delta\nu_G$) of this peak between the stressed graphite anode and the pristine graphite powder. To determine the G peak's wavenumber (ν_G) value for unstressed graphite, ten Raman spectra were randomly collected with a relatively broad laser beam (50× objective) on pristine graphite powder. Fig. 1 shows four typical spectra picked out from those collected spectra data. It can be seen that the Raman spectra of pristine graphite powder show good consistency and ν_G narrowly ranges from 1580.3 cm^{-1} to 1581.2 cm^{-1}. The mean value of those ν_G, 1580.6 cm^{-1}, is thereafter used as reference value for graphite with stress free. Fig. 2A shows micro-Raman mapping of G peak shift ($\Delta\nu_G$), which were collected on graphite anode just after being calendering to an electrode density of 1.7 g cm^{-3}. The corresponding mapping area is indicated

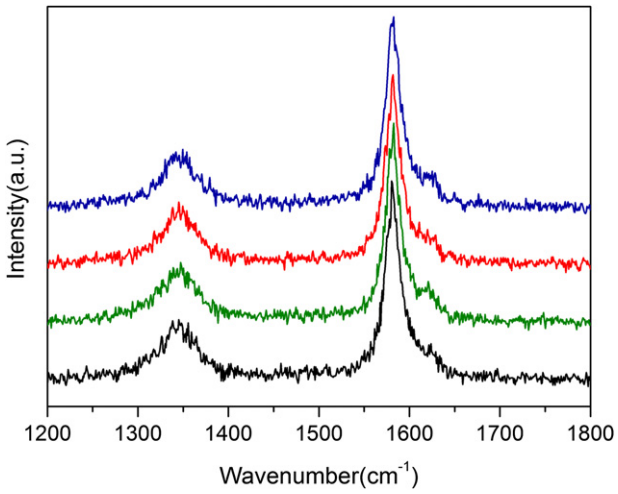

Fig. 1. Four typical Raman spectra randomly collected on pristine graphite powder with a relatively broad laser beam (50× objective).

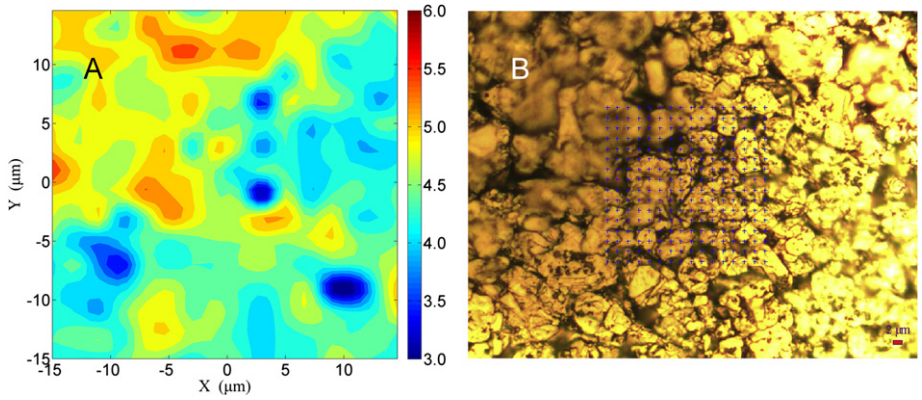

Fig. 2. (A) Micro-Raman mapping of G peak's wavenumber shift collected on graphite anode with an electrode density of 1.7 g cm^{-3}. The *X*/*Y*-axis and the color bar denote the Raman mapping area and the scale of G peak's wavenumber shift, respectively. (B) Optical image of corresponding mapping area on graphite anode.

in Fig. 2B marked with crosses. The map reveals that relatively large compressive stress exists in anode after being rolled as the entire $\Delta\nu_G$ are positive and its average value is as large as 4.6 cm^{-1}. It is also explicit from the map that the distribution of compressive stress in rolled graphite anode is nonuniform. Apparently, the compressive stress is introduced into anode by the calendering process. By calendering process, the SBR particles is forced to cohere tightly to the deformed graphite powder, which restrict the spring back of compressed graphite and consequently lead to compressive stress in graphite anode. Due to the irregular shape and size, the sharp edge and heave of graphite particle must endure larger pressure during calendering process. Consequently, as shown in Fig. 2A, larger stress distributes along the edges and heaves of graphite particle.

The G peak shift of graphite anodes with various electrode densities, i.e., 1.6 g cm^{-3} and 1.8 g cm^{-3}, is mapped in Fig. 3. Coupled with the data in Fig. 2A, it can be easily concluded that the G peak shifts to more positive position with increase of electrode density.

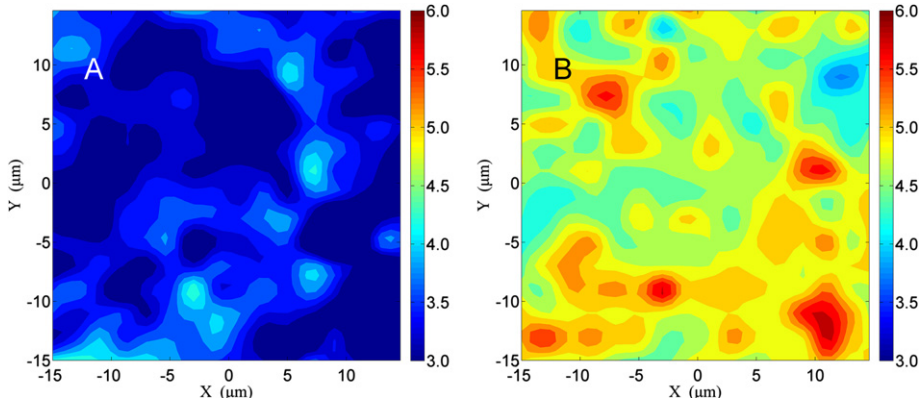

Fig. 3. Micro-Raman mapping of G peak's wavenumber shift collected on graphite anode with an electrode density of (A) 1.6 g cm^{-3}, and (B) 1.8 g cm^{-3}. The *X*/*Y*-axis and the color bar denote the Raman mapping area and the scale of G peak's wavenumber shift, respectively.

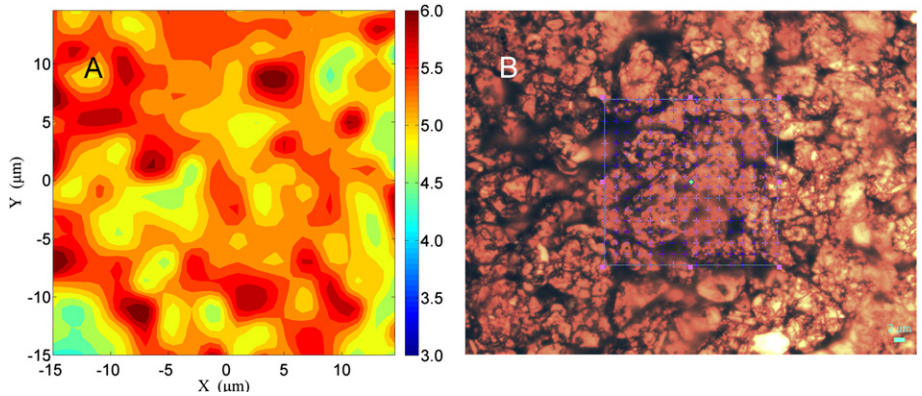

Fig. 4. (A) Micro-Raman mapping of G peak's wavenumber shift collected on graphite anode after 100 charge/discharge cycling. The *X*/*Y*-axis and the color bar denote the Raman mapping area and the scale of G peak's wavenumber shift, respectively. (B) Optical image of corresponding mapping area on graphite anode.

Moreover, inhomogeneous stress distribution appears again in every graphite anode. That phenomenon provides solid evidence that G peak shift of graphite anode is closely dependent upon stress.

The stress characteristic of graphite anode undergone 100 cycles is mapped in Fig. 4A and its corresponding mapping area is depicted in Fig. 4B. The stress of graphite anode during cycle shows similar characteristics with that of graphite anode just after being rolled. That is, only compressive stresses distribute nonuniformly in graphite anode. However, G peak shift of cycled anode, i.e., 5.3 cm^{-1}, is somewhat larger than that of rolled electrode, indicating that additional stress is generated during cycling process. That additional stress is thought to originate from the mutual compression between graphite particles during charge process by volume expansion caused by Li insertion. Furthermore, the volume expansion of graphite particle will be partly restrained by the cohered binder, current collector, and package foil, which also contributes to the stress generation. It is supposed that the stress generated in cycling process cannot be totally restrained either by the soft aluminum package of pouch cell or by the binder due to their poor mechanical strength. So, the compressive stress will be released less or more during cycling process. As a result of stress release, graphite particles deviate from each other and pores and gaps between them become larger, and consequently the thickness of graphite anode increases during cycling process.

3.2. Stress variation of graphite anode in production and cycling process

Fig. 5 shows the stress maps of graphite anode in the process of both fabrication and charge–discharge cycling process. Coupled with the results in Figs. 2 and 4, a comprehensive knowledge of the characteristics and variations of stresses in anode during manufacturing and cycling process is obtained. As described above, relatively big compressive stress ($\Delta\nu_G = 4.6$ cm^{-1}) is introduced into graphite anode by the rolling process. That compressive stress is reduced by the subsequent vacuum baking as $\Delta\nu_G$ decreases to 2.1 cm^{-1}. One charge–discharge cycling just slightly raise the stress ($\Delta\nu_G = 3.0$ cm^{-1}). However, the stress in graphite anode accumulates to a high level after 100 charge–discharge cycling ($\Delta\nu_G = 5.3$ cm^{-1}). That stress accumulation seems to slow down or even keep constant in the latter cycling as $\Delta\nu_G$ of 200 and 350 cycled graphite anode is 5.5 cm^{-1} and 5.0 cm^{-1}, respectively. This stress variation distinctly reveals that the stress generation and accumulation mainly occur at the early stage of cycling.

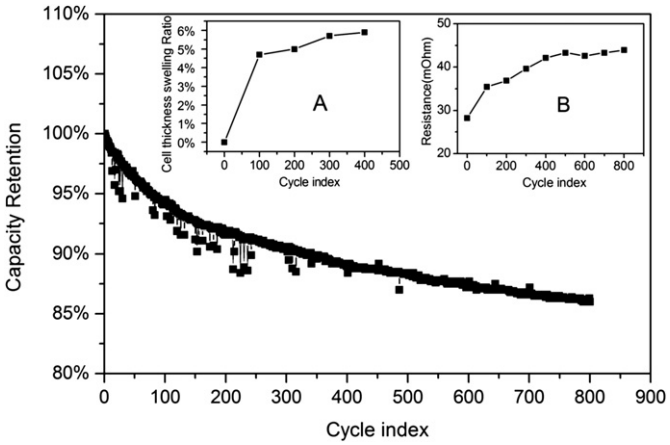

Fig. 6. A typical capacity fading curve of pouch cell at a charge/discharge current of 1.4 A/1.0 A at 45 ± 1 °C. Inset A shows thickness swelling ratio of pouch cell and inset B depicts the resistance variation of pouch cell along the charge/discharge cycling process.

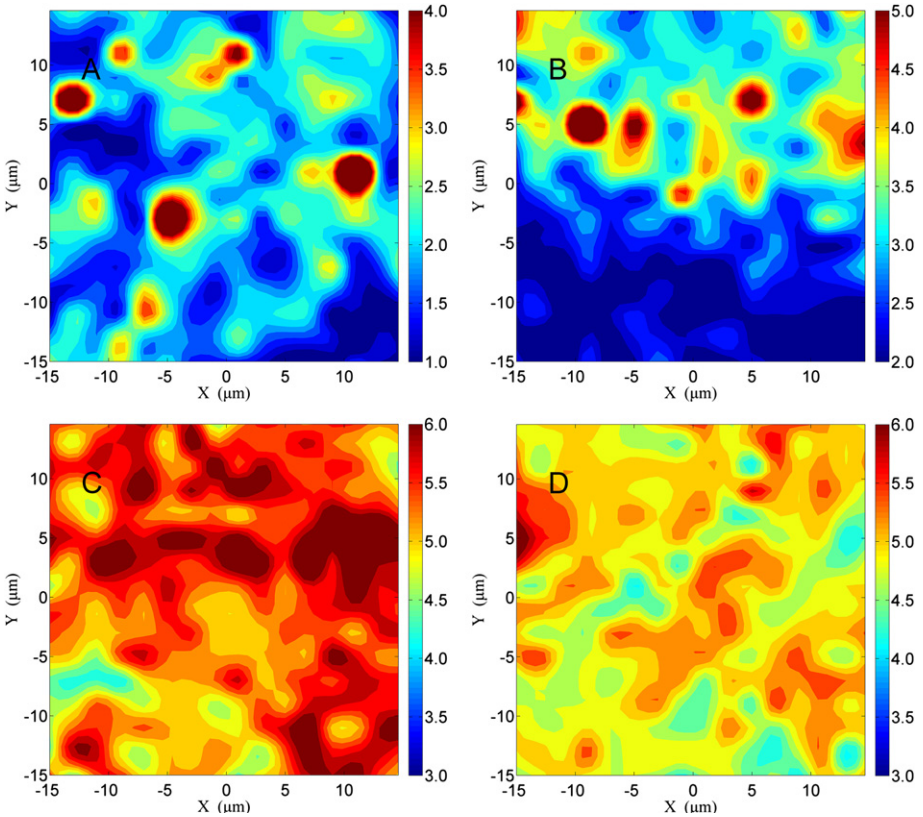

Fig. 5. Micro-Raman mapping of G peak's wavenumber shift collected on graphite anode undergone (A) vacuum baking, (B) 1 cycle, (C) 200 cycles, (D) 350 cycles. The *X*/*Y*-axis and the color bar denote the Raman mapping area and the scale of G peak's wavenumber shift, respectively.

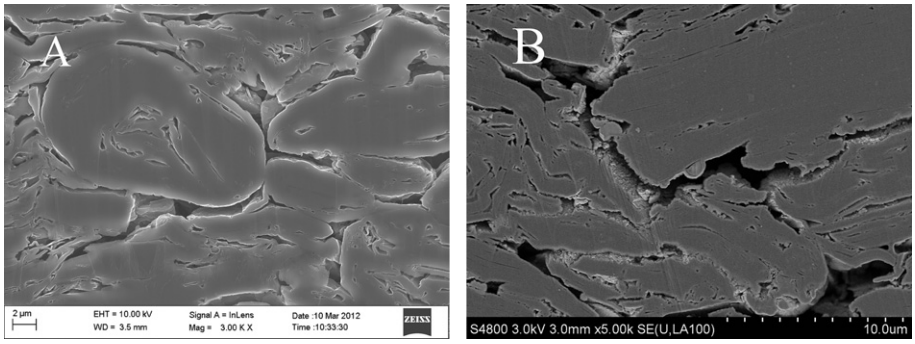

Fig. 7. Cross-section of graphite anode (A) before cycling and (B) after 100 charge/discharge cycling at 45 ± 1 °C.

3.3. Correlation of stress characteristic of graphite anode with cycle life of pouch LIB

As shown in Fig. 6, the as-fabricated pouch cell possesses excellent cycle stability. The capacity retention of the pouch cell is still larger than 85% even after 800 charge/discharge cycles under elevated temperature (45 ± 1 °C). However, a close inspection of the curve finds that the capacity fading is relatively fast in the earliest 100 cycles and then slows down in the latter cycles. Two factors, namely, remedy of SEI and deterioration of electrical contact of graphite particles from current collector during cycling process, are commonly accepted reasons for the capacity fading of graphite electrodes in Li-ion cells [22–24]. However, the fast capacity loss in earliest 100 cycles suggests that SEI remedy and deterioration of electrical contact proceed more seriously in this stage than in the latter cycling. Coupled with the stress variation of graphite anode shown in Fig. 5, the root cause of the serious SEI remedy and deterioration of electrical contact of graphite anode in the earliest cycling is ascribed to the big compressive stress generation and accumulation in this stage. At first, the release of compressive stress causes the volume expansion of graphite anode and eventually weakens the electrical contact of the graphite particles with the current collector. As can be seen from Fig. 6 (inset A), in agreement with stress variation trend in Fig. 5, steep thickness swelling of pouch cell happens in the early stage of cycling. One should keep in mind that cathode almost keep its original state in cycling due to its nearly zero strain during Li-insertion/extraction. So, the cell swelling almost originates from the anode expansion. It is the steep anode expansion which causes rapid deterioration of electrical contact of the graphite particles with the current collector. This suggestion is clearly verified by the cell resistance variation (inset B in Fig. 6) as the resistance increase in the earliest 100 cycles is faster than that in the latter. Secondly, stress damages graphite particles in anodes during cycling process. As shown in Fig. 7A, the graphite particle in anode shows relatively good integrity before charge–discharge cycling and most of pores/cracks in its interior are closed. However, due to larger stress generated and accumulated in the early cycling stage, some graphite particles are broken and even totally disintegrated after 100 cycles at 45 °C (Fig. 7B). In that case, many pores and cracks in the inner of graphite particle are exposed to electrolyte. Consequently, SEI formation takes place in those fresh surfaces and the cell loses partial capacity.

4. Conclusions

MRS technique is a useful tool to probe the stress in graphite anode of commercial pouch cell during the process of manufacturing and prolonged cycling on a microscopic scale. This technique reveals that the stress in graphite anode is always compressive and its distribution is inhomogeneous. The compressive stress is firstly introduced to anode by rolling process and cannot be fully eliminated by the subsequent vacuum baking treatment. Stress generation and accumulation mainly occur at the early stage of cycling but slows down at the latter cycling. As a result, the release of compressive stress causes faster thickness swelling of graphite anode in this stage, which eventually leads to rapid deterioration in the electrical contact of the graphite particles with the current collector. As well as thickness increase, stress in graphite anode causes the graphite particle to be cracked or even degraded, which expose fresh surface to electrolyte. The SEI formation in those fresh surface results in irreversible capacity loss. The electrical contact deterioration and SEI formation in the earliest cycling process together cause the fast capacity fading in this stage. Those results imply that the battery manufacturer should elaborately optimize manufacturing process and carefully select graphite material to reduce or eliminate the stress in anode so as to reduce cell swelling and prolong cycle life.

References

[1] E. Markervich, G. Salitra, M.D. Levi, D. Aurbach, J. Power Sources 146 (2005) 146–150.
[2] R. Kostecki, F. McLarnon, J. Power Sources 119 (2003) 550–554.
[3] X. Wang, Y. Sone, S. Kuwajima, J. Electrochem. Soc. 151 (2004) A273–A280.
[4] Y. Yi, C. Wang, A.M. Sastry, J. Eng. Mat. Technol. 128 (2006) 73–80.
[5] Y. Cheng, M.W. Verbrugge, J. Power Sources 190 (2009) 453–460.
[6] X. Zhang, W. Shyy, A.M. Sastry, J. Electrochem. Soc. 154 (2007) A910–A916.
[7] J. Christensen, J. Newman, J. Solid State Electrochem 10 (2006) 293–319.
[8] S. Renganathan, G. Sikha, S. Santhanagopalan, R.E. White, J. Electrochem. Soc. 157 (2010) A155–A163.
[9] A. Mukhopadhyay, A. Tokranov, K. Sena, X. Xiao, B.W. Sheldon, Carbon 49 (2011) 2742–2749.
[10] V.A. Sethuraman, M.J. Chon, M. Shimshak, V. Srinivasan, P.R. Guduru, J. Power Sources 195 (2010) 5062–5066.
[11] V.A. Sethuraman, N. Van Winkle, D.P. Abraham, A.F. Bower, P.R. Guduru, J. Power Sources 206 (2012) 334–342.
[12] M.S. Amer, Int. J. Solids Struct. 42 (2005) 751–757.
[13] G. Sarau, M. Becker, S. Christiansen, 24th European Photovoltaic Solar Energy Conference, 21–25 September 2009, Hamburg, Germany.
[14] T. Kunz, M.T. Hessmann, B. Meidel, C.J. Brabec, J. Cryst. Growth 314 (2011) 53–57.
[15] I.D. Wolf, Semicond. Sci. Technol. 11 (1996) 139–154.
[16] H. Ichimaru, G. Pezzott, Mater. Sci. Eng. A 326 (2002) 261–269.
[17] C.J. Lee, G. Pezzotti, Y. Okui, S. Nishino, Appl. Surf. Sci. 228 (2004) 10–16.
[18] S. Reich, C. Thomsen, Phil. Trans. R. Soc. Lond. A 362 (2004) 2271–2288.
[19] A.M. Gigler, A.J. Hube, M. Bauer, A. Ziegler, R. Hillenbrand, R.W. Stark, Opt. Express 17 (25) (2009) 22351–22357.
[20] N. Melanitis, P.L. Tetlow, C. Galiotis, S.B. Smith, J. Mater. Sci. 29 (1994) 786–799.
[21] C. Galiotis, D.N. Batchelder, J. Mater. Sci. Lett. 7 (1988) 545–548.
[22] D. Aurbach, J. Power Sources 119 (2003) 497–503.
[23] D. Aurbach, M.D. Levi, E. Levi, A. Schechter, J. Phys. Chem. B 101 (1997) 2195–2206.
[24] R. Yazami, Electrochim. Acta 45 (1999) 87–97.